Live Stimulated Raman Histology for the Near-Instant Assessment of Central Nervous System Samples

Romain Appay, Barbara Sarri, Sandro Heuke, Sébastien Boissonneau, Chang Liu, Etienne Dougy, Laurent Daniel, Didier Scavarda, Henry Dufour, Dominique Figarella-Branger, et al.

Live Stimulated Raman Histology for the near-instant assessment of central nervous system samples

Romain Appay[1,2,3,*], Barbara Sarri[3,4], Sandro Heuke[3], Sébastien Boissonneau[5], Chang Liu[4], Etienne Dougy[6], Laurent Daniel[1,6], Didier Scavarda[7], Henry Dufour[5], Dominique Figarella-Branger[1,2], Hervé Rigneault[3,4]

[1]APHM, CHU Timone, Service d'Anatomie Pathologique et de Neuropathologie, Marseille, France.

[2]Aix-Marseille Université, CNRS, INP, Inst Neurophysiopathol, Marseille, France.

[3]Aix-Marseille Université, CNRS, Centrale Marseille, Institut Fresnel, Marseille, France

[4]Lightcore Technologies, Marseille, France

[5]Neurosurgical Department, Aix-Marseille University, APHM, CHU Timone, France.

[6]APHM Timone Hospital, Biological Resource Center – Tumorbank and Bank of Muscles (TBM)

[7]Department of Pediatric Neurosurgery, APHM, Timone Hospital, Marseille, France.

Corresponding authors:

e-mail address: romain.appay@ap-hm.fr ; herve.rigneault@fresnel.fr

Abstract

Central nervous system tumors encompass many heterogeneous neoplasms with different outcomes and treatment strategies. The current classification of these tumors is based on molecular parameters in addition to histopathology to define tumor entities. This genomic characterization of tumors is also becoming increasingly essential for physicians to identify targeted therapy options. The deployment of such genomic profiling relies on an efficient surgical sampling. To perform an appropriate tumor resection and a correct sampling of the tumor, the neurosurgeon may request an intraoperative pathological consultation. Stimulated Raman histology (SRH), an emerging non-destructive imaging technology, can address this challenge. SRH allows for a rapid and label-free microscopic examination of unprocessed tissues samples in near-perfect concordance with standard histology. In this study we showed that SRH enabled the near-instant microscopic examination of various central nervous system samples without any tissue processing such as labelling, freezing nor sectioning. Since SRH imaging is a non-destructive approach, we demonstrated that the tissue could be readily recovered after SRH imaging and reintroduced into the conventional pathology workflow including immunohistochemistry and genomic profiling to establish a definitive diagnosis.

Keywords: central nervous system; brain tumors; stimulated raman histology; intraoperative consultation; histopathology; label-free;

Introduction

Central nervous system (CNS) tumors are a challenge for public-health systems worldwide due to their increasing incidence in recent decades[1,2]. CNS tumors include many different neoplasms, including primary and metastatic tumors, with different outcomes and require different treatment strategies. Primary CNS tumors are the most common pediatric solid tumors and constitute the leading cause of cancer-related morbidity and mortality in childhood[3]. In adults, the majority of CNS tumors are metastases from systemic cancer while meningiomas and high grade glial tumors account two-thirds of all primary brain tumors[4,5].

The latest advances in genome sequencing technology and large-scale genome research have considerably improved our understanding of cancer-associated genomic alterations. Our deepened understanding contributes to more accurate tumor classification and was the basic concept of the revised fourth classification of tumors of the central nervous system (CNS) published by the WHO in 2016 while introducing the concept of "integrated diagnosis"[6]. In line with this classification and based on the work of the Consortium to Inform Molecular and Practical Approaches to CNS Tumor Taxonomy, the recently published 2021 fifth edition further supported the role of molecular diagnostics in CNS tumor classification[7]. In addition, the genomic characterization of tumors are also becoming increasingly essential for physicians to identify targeted therapies options[8]. Following these WHO's guidelines, many tumors require additional molecular evaluation in addition to the conventional pathology workflow. Deploying such a diagnostic genomic profiling constitutes one of the seven major challenges to cure brain tumors according to recently published an expert committee Position Paper[9]. The quality of the surgical specimen sent for histopathological and further molecular studies is therefore of major importance.

That being said, the two main objectives of the neurosurgical procedure are (i) performing an appropriate tumor resection while (ii) achieving a correct sampling of the tumor for an effective subsequent pathological diagnosis. To meet these objectives, the neurosurgeon may request a quick preliminary sample analysis of the pathologist, a procedure called intraoperative consultation (IC). The appropriate surgical tumor resection depends on the tumor type. Indeed, solitary brain metastasis or meningioma require a complete surgical resection[10,11]. Similarly, a high grade glioma will benefit from a maximal extend of surgical resection[12–16]. Conversely, in patients with CNS lymphoma, surgical resection is not desirable in favor of chemotherapy[17]. In this context, an IC is often requested to suggest a preliminary diagnosis that decides over the continuation of the surgery and will guide the extent of surgical resection. The effective sampling of the tumor might be particularly challenging when the tumor location is difficult to reach for the neurosurgeon. In this case, the current strategy to reduce the risk of non-relevant sampling includes an IC to assess the presence of tumor cells. The IC is therefore decisive to provide neurosurgeon with quick diagnostic information that may affect the surgical procedure.

Currently, the standard IC involves cytological preparations, or less frequently frozen sectioning, followed by hematoxylin & eosin (HE) staining for histopathological examination. Such techniques are time-consuming which is detrimental considering that longer durations of surgeries are associated with potential complications[18]. In addition, these conventional histopathological approaches inevitably lead to the depletion of a precious tumor material[19]. An alternative technique that would provide reliable diagnostic information without tissue consumption, allowing its use for further studies, would constitute a game changer in intra-surgery guidance.

Stimulated Raman histology (SRH) is an emerging technology that resulted from the work of Xiaoliang Sunney Xie in the field of label free coherent Raman imaging. SRH allows for a rapid, label-free and non-destructive

microscopic examination of unprocessed samples in near-perfect concordance with standard histology[20–23]. SRH is based on the ability to detect chemical molecular bonds in tissues owing to the interaction between molecular vibrations and the laser light[24]. Imaging simultaneously both the CH2 and the CH3 chemical bond distribution within a tissue, SRH enables to generate virtually colored images mimicking HE staining[20,25].

In this study, we demonstrated the performance of Stimulated Raman Histology (SRH) to perform a near-instant microscopic examinations of various central nervous system samples. SRH investigation was followed by the recovery of all the SRH imaged samples for conventional histopathology workflow including microscopic morphology, immunohistochemistry, and genomic profiling.

Material and methods

Central nervous system samples selection and preparation

Ten frozen samples amongst which one normal brain sample and 9 of the most common CNS tumor types were retrieved from the APHM tumor bank CRB TBM. The neoplastic samples included 2 gliomas (1 low grade glioma and 1 high grade glioma), 2 meningiomas (1 transitional meningioma and 1 anaplastic meningioma), 1 lymphoma (diffuse large B cell lymphoma primary of the central nervous system), 1 pituitary adenoma, 1 medulloblastoma, and 2 metastatic tumors (1 adenocarcinoma and 1 squamous cell carcinoma). All patients gave their written consent and protocols were approved by the APHM under the supervision of CRB TBM (N°DC2013-1781). These retrieved samples, initially snap-frozen and stored in vapor phase nitrogen tank, were thawed at room temperature for a few minutes. A small, approximately 5 cubic millimeters, specimen of each sample was placed between two coverslips to perform SRH imaging. This required less than one minute of preparation. Following SRH imaging, all samples were recovered and routinely processed in the APHM pathology department as illustrated in Figure1.

Stimulated Raman Histology

To perform SRH, stimulated Raman scattering (SRS) images of both CH2 and CH3 bonds were acquired simultaneously with the BondXplorer commercial SRS microscope (Lightcore Technologies), as described in Heuke et al[26]. Briefly, a 3-color laser system (1-2ps, 793 nm, 1024nm, 1033nm, 80MHz – deltaEmerald APE) was used for excitation of SRS matching the Raman resonances at 2845cm^{-1} (CH2) and at 2930cm^{-1} (CH3), respectively. The three beams entered an SRS laser scanning microscope (BondXplorer, Lightcore Technologies) and were focused onto the sample using a water immersion objective lens. Laser powers at the sample plan were ~30mW from each beam. The microscope was controlled with the open-source software 'Scan-image' which allowed to set the pixel dwell time (dt), pixel number (pn), field of view (fov) and accumulation (acc) over a wide range. Two modalities, available in the BondXplorer microscope, were used in this study. In the first modality, called 'Live SRH', the user could freely navigate (in x y z directions) within the sample in real time (dt=5µs, acc=1, fov=214µm², pn=512 or 1024) to identify regions of interest. In the second modality, called 'Mosaic SRH', millimeter sized images were acquired by stitching smaller images next to each other. For the mosaic image acquisition ('mosaic SRH'), the x y z coordinates were pre-determined using and the 'Live SRH' modality. The parameters (fov, dt, pn) for the 'mosaic SRH' acquisition were set as follow: dt=5µs, acc=1, fov=214µm², pn=1024. A fully automatic coloring algorithm was developed to generate, starting from the vibrational CH2 and CH3 images, a three-channel RGB image with color mimicking a conventional HE staining.

Conventional histopathology

Following SRH imaging, the sample were recovered from between the coverslips and fixed in 4% formalin for 24 hours. The specimens were then included in a conventional pathology workflow comprising paraffin embedding, sectioning and HE staining. Immunochemistry was performed on the Benchmark Ventana autostainer (Ventana Medical Systems SA, Illkirch, France) with routinely used antibodies targeting AE1-AE3 (Polyclonal, Roche), Bcl6 (PG-B6p, Dako), CD10 (56C6, Dako), CD20 (L26, Cliniscience), CD3 (Polyclonal, Dako), CD56/NCAM (123C3, Roche), CDX2 (DAK-CDX2, Dako), Chromogranin (DAK-A3, Dako), CK20 (Ks20.8, Dako), CK5/6 (DS/16B4, Dako), CK7 (OV.TL12/30, Menarini), EGFR (3C6, Roche), EMA (E29, Dako), Filamin (PM6/317, Interchim), FSH (Polyclonal, Roche), GATA3 (L50-823, Roche), GFAP (6F2, Dako), IDH1 R132H (H09, Clinisciences), Ki67 (Mib-1, Dako), MUM1 (MUM1P, Dako), NeuN (A60, Millipore), Neurofilament (2F11, Sigma-Aldrich), OLIG2 (EP112, Diagomix), P63 (4A4, Roche), PS100 (Polyclonal, Dako), RP (1/E2, Roche), SSTR2 (UMB1, Abcam), Synaptophysin (DAK-SYNAP, Dako), TTF1 (8G7G3/1, Dako). The slides were scanned using the Hamamatsu Nanozoomer system 2.0-HT and the presented images were obtained using the NDP.view2 viewing software (ver 2.6.17).

DNA extraction and quantification

DNA was extracted from four 3.5 µm thick tissue section using the IDXTRACT-mag-FFPE kit (ID-Solutions, Grabels France) coupled to the automaton (IDEAL-32, ID-Solutions) as per the manufacturer's guidelines. DNA was quality checked and quantified using DNA calibrated by an external standard range using the IDQUANTq kit (ID-Solutions) and the Mic® quantitative PCR instrument (Bio Molecular Systems, Queensland, Australia).

Targeted next-generation DNA sequencing and mutational analysis

Mutational analysis was performed using the Ion S5™ XL next-generation sequencing system (Thermo Fisher Scientific) targeting the following gene panel: *AKT1, ATRX, BRAF, CDKN2A, CIC, EGFR, FGFR1, H3F3A, HIST1H3B, IDH1, IDH2, NOTCH1, PIK3CA, PIK3R1, PTEN, PTPN11, TERT, TP53.*

DNA methylation analysis and data processing

DNA bisulfite conversion was performed using the ZymoEZ DNA methylation kit (Zymo research, USA), then treated with FFPE DNA Restore kit (Illumina, San Diego, CA, USA) and DNA clean and concentrator-5 (Zymo research, USA). Standard quality controls confirmed DNA quantity/quality and bisulfite conversion. The DNA was then processed using the Illumina Infinium HumanMethylation EPIC Bead-Chip array (Illumina, San Diego, CA, USA) according to the manufacturer's instructions. The iScan control software was used to generate raw data files from the BeadChip in .idat format and analysed using GenomeStudio version 2.0 (Illumina, San Diego, CA, USA) with regard to quality measures according to the manufacturer's instructions. The .idat files were uploaded to the online CNS tumor methylation classifier platform https://www.molecularneuropathology.org and a report was generated, providing prediction scores (calibrated score) for DNA methylation classes according to the version 12.5 of the classifier [27].

Results

'Live' imaging of CNS samples

We first designed a 'Live SRH' imaging mode allowing to rapidly explore the sample and to delineate the regions of interest necessary to guide a larger area acquisition. Once under the BondXplorer microscope in the 'Live SRH' mode, a virtually stained image corresponding to an area of 214x214µm could be observed almost instantaneously. This fast-imaging approach was used to perform a microscopic examination along the two horizontal axes (x,y) but also in depth (z) to screen different areas of the observed sample (Figure 1). Supplementary video 1 shows the 'Live SRH' operation mode for the microscopic histology exploration of each tumor sample.

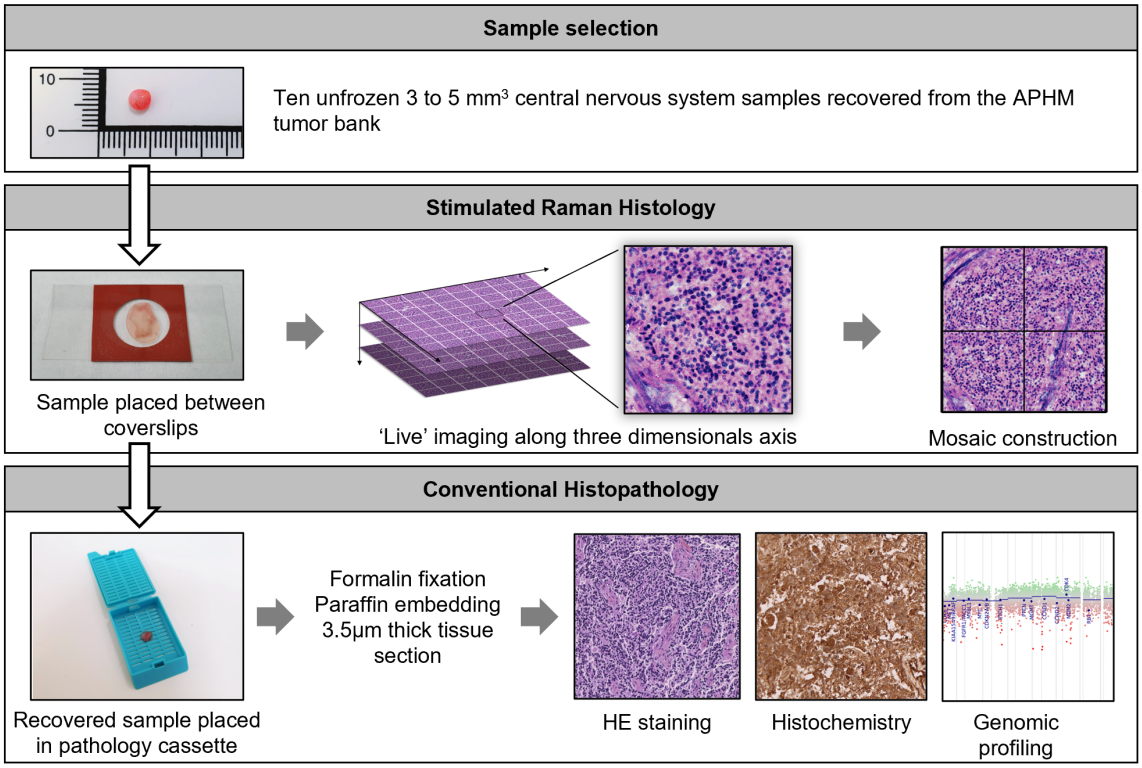

Figure 1: Study Design: Unfrozen central nervous system samples were placed between coverslips for Stimulated Raman Histology imaging then recovered and included in a conventional histopathology workflow.

As illustrated in Figure 2, this live SRH observation permitted the identification of characteristic features of different tumor types, allowing for a preliminary diagnosis. The examination of the normal brain sample revealed a normal texture of the neuropil associated with scattered glial cells and neurons. On the other hand, in the low-grade glioma sample, the neuropil was altered by a proliferation of slightly piloid tumor cells without frank cytonuclear atypia nor microvascular proliferation. A diagnosis of high-grade glioma could be assessed for the third case demonstrating a highly cellular tumor with marked nuclear pleomorphism and microvascular proliferation. Regarding meningiomas, the characteristic microscopic appearance of sheets of tumor cells with indistinct cell borders arranged in a whorled or lobulated architecture could be recognized. The benign meningioma demonstrated regular round to oval monomorphic nuclei with some appearing to have nuclear pseudoinclusions

whereas the aggressive meningioma demonstrated increased cellularity nuclear pleomorphism. Medulloblastoma could be recognized as a proliferation of undifferentiated small round-shaped relatively uniform cells with hyperchromatic nuclei focally arranged around a central area of neuropil corresponding to the characteristics Homer-Wright rosettes of this tumor. We could also identify the relatively monomorphic proliferation of large cells with round to oval irregular nuclei with distinct nucleoli corresponding to the centroblasts or immunoblast cytology of the diffuse large B cells. Pituitary adenoma could be recognized by the trabecular architecture of monomorphic cells with round nuclei, inconspicuous nucleoli, and moderate degree of nuclear pleomorphism. Finally, cohesive sheet or island of atypical cells could be observed in both metastatic carcinomas. Abortive tubule formations were seen in the adenocarcinoma whereas large polygonal malignant cells containing keratin were observed in the squamous cell carcinoma.

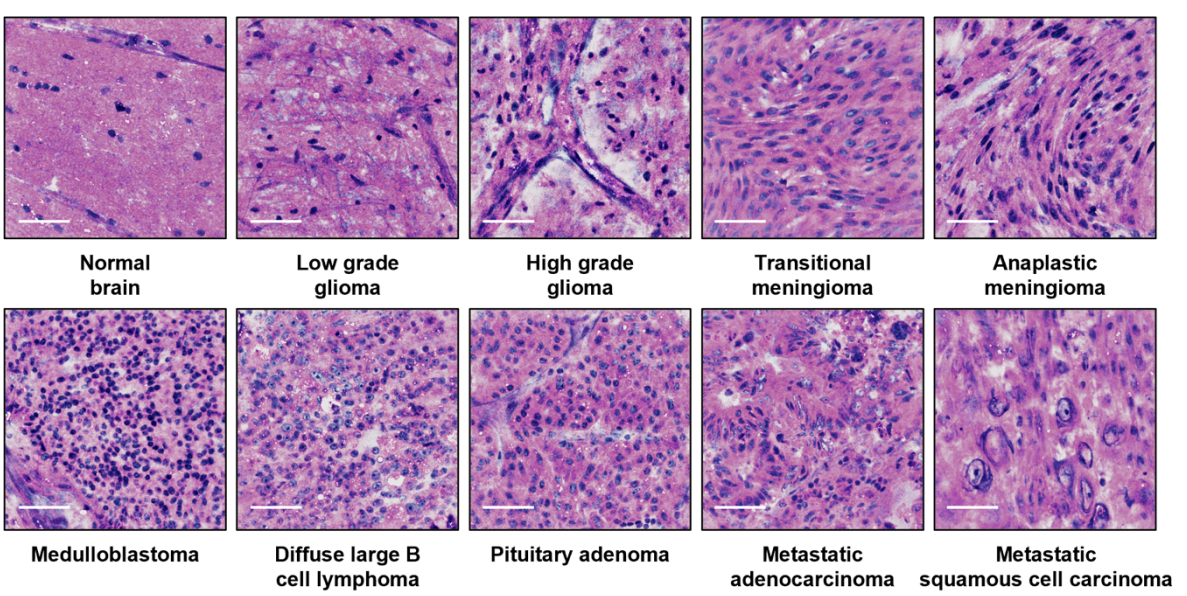

Figure 2: 'Live SRH' examination of CNS samples: The fast-imaging approach permitted the identifications of characteristics features of different tumor types. Scale bars corresponds to 50µm.

'Mosaic' large images acquisition

To visualize a larger area of the sample, we used the BondXplorer 'mosaic SRH' modality where several small SRH images were adjacently acquired and positioned within a 2D-grid. The size of the desired area depended on the number of single field of view acquired which was linked to the total acquisition time of the constructed image (Figure 3). As illustrated in Figure 4, the larger mosaic SRH image permitted for an improved assessment of the whole sample as well as the general architecture of the different tumor types. Whereas gliomas and lymphoma were characterized by a diffuse architecture, the other tumor types demonstrated specific pattern of cellular organization. The trabeculae of pituitary adenoma, the large nodules of the medulloblastoma, the syncytial whorled architecture of meningioma as well as the recognition of cohesive islands characteristic of carcinoma metastases was greatly facilitated in comparison to live imaging.

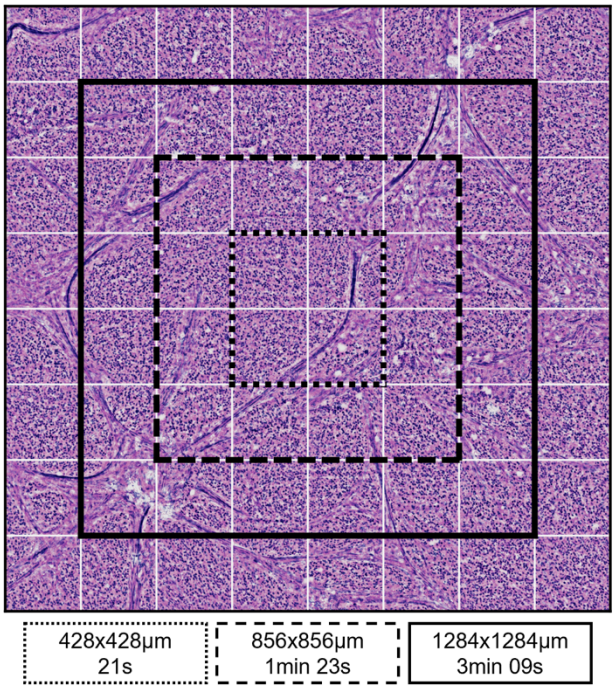

Figure 3: Mosaic construction: Several 'Live SRH' images were adjacently acquired and positioned within a 2D-grid to visualize a larger area of the sample. The total acquisition time varied depending on the size of the desired area. One square corresponds to an area of 214x214µm. Abbreviations: min: minutes, s: seconds.

Subsequent use of the SRH imaged sample in conventional histopathology workflow

We then aimed to demonstrate the compatibility of SRH with a conventional histopathological examination of tissues. All the samples could be retrieved from between the coverslips for tissue processing including formalin fixation, paraffin-embedding, HE staining, immunohistochemistry and molecular biology (Figure 4). For each sample, although the microscopic aspect observed were altered by freezing artifacts due to the initial storage in nitrogen, the histopathological aspect of the different tumor types could be easily recognizable and was in accordance with the expected tumor type. Of importance, histopathological findings were comparable to those previously observed on the same samples with SRH (Figure 4). All the immunostaining performed were informative and in accordance with the results obtained on the routinely processed samples. Of note, this included a large panel of antibodies targeting membranous, cytoplasmic as well as nuclear proteins. Additional molecular studies were performed for two cases. Targeted next-generation DNA sequencing and mutational analysis of the high grade glioma revealed a *TERT* promotor mutation (c.1-124C>T) associated with *PTEN* mutation (c.1007dup (p.Tyr336Ter)) and *EGFR* amplification without *IDH1* nor *IDH2* mutation in accordance with the diagnostic of glioblastoma, *IDH*-wildtype. The DNA methylation analysis performed on the medulloblastoma demonstrated a methylation profile of medulloblastoma, SHH-activated according to the version 12.5 of the classifier (score 0.99) in accordance with the expected result. Altogether, a histopathological diagnosis including immunohistochemistry and genomic profiling could be successfully established for all cases retrieved following their first assessment with SRH.

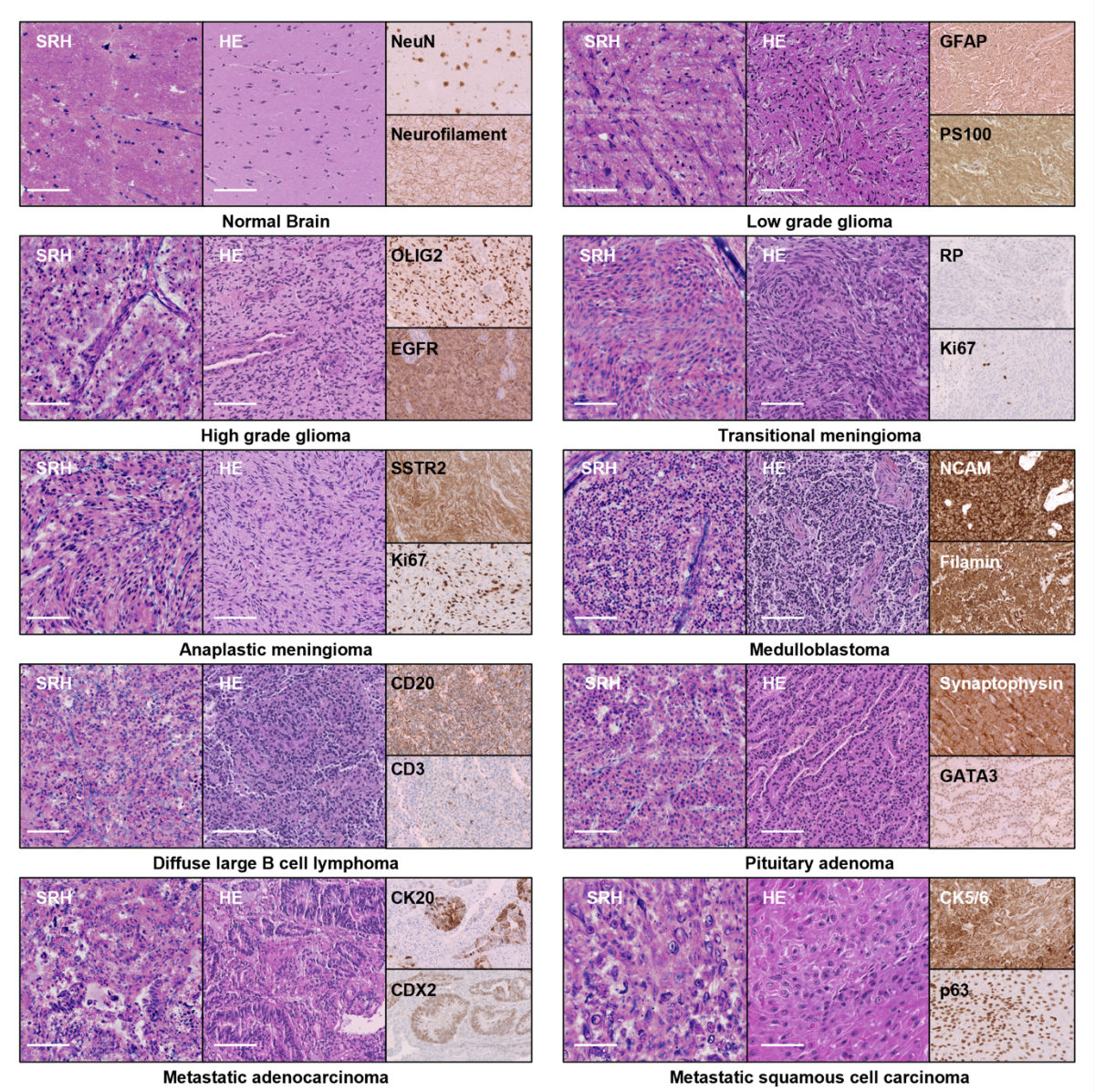

Figure 4: "Mosaic' large image acquisition and subsequent use of the samples in a conventional pathology workflow: All the samples were retrieved and processed in a conventional pathology workflow. 'Mosaic SRH' permitted for an improved assessment of the samples with histopathological aspects comparable to those observed with hematoxylin and eosin staining. Two representatives' immunostaining are presented for each sample. Scale bars corresponds to 100µm

Discussion

In this study, we demonstrated the relevance of stimulated Raman histology (SRH) for rapid microscopic examination of various central nervous system samples without any tissue processing such as labelling, freezing nor sectioning. As a non-destructive approach, this novel label free imaging modality enabled us to recover the imaged samples and to include them in a conventional pathology workflow including formalin fixation, paraffin embedding HE staining and genomic profiling (using targeted next generation sequencing and methylation profile

analysis). The BondXplorer SRH microscope allowed for the 'Live SRH' modality and meaningful microscopic examination of CNS samples followed by the subsequent larger 'mosaic SRH' imaging of the whole sample to establish a definitive histopathological diagnosis including immunohistochemistry and molecular biology.

SRH relies on stimulated Raman scattering imaging of CH2 and CH3 molecular groups within the tissue sample. Subsequent coloring of the obtained images can exquisitely mimic HE staining for the direct reading and interpretation by pathologists following their current manner to examine histological HE-stained slides under a microscope. As such SRH imaging can be directly accepted by pathologist. Previous studies demonstrated SRH's suitability for the analysis of freshly excised CNS surgical specimens which is particularly valuable for intraoperative pathological consultations [20–23,28–30]. Indeed, the current workflow for IC requires the sample transport to a pathology department, processing of the specimen including cytological preparations (smear or touch preps) and/or frozen sections, both associated with rapid HE staining of the slides and their interpretation by a neuropathologist[19]. This conventional procedure takes 20-30 minutes for each sample to be processed [31] with potential negative impact for the patient since an increase surgery duration is associated with possible complications [18]. Moreover, as this conventional procedure is time consuming, it cannot be used repeatedly to assess multiple surgical resection margins. SRH constitutes an interesting alternative as it provides rapid microscopic images of freshly excised tissues samples. In our study, a near instantaneous and informative histopathological examination could be performed on all analyzed samples. Furthermore, among the different approaches of specimen processing for an IC, cytological preparations allow pathologists to study the cellular characteristics of the tumor cells but the overall histopathological architecture of the tissue is lost whereas frozen sectioning preserves the underlying tissue architecture but may induce major freezing and sectioning artifacts hindering interpretation[32]. SRH constitutes a freezing-free and sectioning-free approach that facilitates both architecture and cellular analysis on a freshly excised sample. As previously reported[21,22,33], we confirm within our study that the SRH examination of the samples reveals similar architectural and cellular features as compared to HE images arising from the same sample processed in a conventional pathology workflow. It shall be noted, however, that all the samples analyzed in our study were retrieved from a tumor bank and, therefore, have been somewhat altered by storage in nitrogen as observed on the HE stained section. In addition, the design of our study may impact the interpretation of the results. Indeed, the cases were selected based on the tumor types, and this was therefore known at the time of the SRH image analysis. Although a blinded study is required to validate the diagnostic capability of this approach, the agreement between the observed images and the HE images provides first robust evidence of its effectiveness. To further reduce the examination time, a SRH microscope would have to be integrated into the operating room. Since SRH images are digital by nature, their remote interpretation is readily enabled. Medical centers without local neuropathologist would greatly benefit from SRH imaging for optimal efficiencies of their surgical management. At last, neural networks and artificial intelligence analysis of SRH images may assist the pathologist in making a diagnostic decision as previously reported[21].

An international panel of brain cancer researchers recently identified seven major challenges that must be overcome to cure primary brain tumors and they should serve as the foci for future research and investment. In the context of precision medicine, they discussed the importance of genome-wide classification tools and highlighted the challenge of diagnostic genomic profiling considering the often-limited amounts of tumor material available[9]. Indeed, histopathological examination inevitably leads to the depletion of a valuable diagnostic material. This point might be particularly detrimental for the biopsy acquisition of CNS tumors as the anatomical location,

sometimes difficult to reach for the surgeon, indicates a stereotaxic biopsy to guide the removal of a small amount of tissue for pathological examination. Such a procedure is particularly challenging, and an intraoperative diagnosis is often required for the sole purpose of confirming the correct sampling of the lesion despite the consumption of precious tumor tissue. Of particular interest, we showed in this study that a tissue imaged by SRH could be used *ad integrum* for histopathology and genomic profiling. All samples retained their immunogenic properties for immunohistochemistry as well as their genomic integrity for molecular studies in accordance with previously reported results[20,28]. In this context, an SRH approach would be particularly useful to perform a microscopic evaluation of a sample without depleting precious material for further analysis.

The performances of SRH rely on different strengths: live or quasi-instantaneous imaging of pseudo HE images of a sample without preparation, allowing microscopic examination without material consumption nor alteration. As such, SRH represents a valuable extension in the histopathological arsenal methods whose digital images can be readily interpreted and assessed by pathologists, possibly remotely, or processed by artificial intelligence.

Declarations

Competing interests:

The authors have no competing interests to declare that are relevant to the content of this article.

Funding:

We acknowledge financial support from the Centre National de la Recherche Scientifique (CNRS), ANR grants (ANR-11-IDEX-0001-02, ANR-10-INSB-04-01, ANR-11-INSB-0006, ANR-16-CONV-0001, ANR-21-ESRS-0002 IDEC), INSERM (PC201508, 18CP128-00, 22CP139-00) and Lightcore Technologies. This project has received funding from European Union's Horizon 2020 EU ICT 101016923 CRIMSON and European Research Council (ERC), SpeckleCARS, 101052911. Views and opinions expressed are however those of the authors only and do not necessarily reflect those of the European Union or the European Research Council. Neither the European Union nor the granting authority can be held responsible for them.

Ethics approval and Consent:

The study was conducted according to the guidelines of the Declaration of Helsinki and approved by the Institutional Review Board of APHM under the supervision of CRB TBM (N°DC2013-1781). Informed consent was obtained from all subjects involved in the study.

Data:

The datasets generated during and/or analysed during the current study are available from the corresponding author on reasonable request.

Author Contributions:

R.A., B.S., and H.R. performed study concept and design; R.A., B.S., S.H., and H.R., performed development of methodology and writing, review and revision of the paper; S.B., D.S., H.D., E.D. and L.D. provided samples; R.A. and B.S. performed analysis and interpretation of data; C.L. provided technical and material support. All authors read and approved the final paper.

Acknowledgments:

We thank the APHM Tumor Bank (CRB-TBM, authorization number: DC2013-1781; CRB BB-0033-00097) for collecting and providing tissue samples.

References

(1) Ostrom, Q. T.; Gittleman, H.; Liao, P.; Vecchione-Koval, T.; Wolinsky, Y.; Kruchko, C.; Barnholtz-Sloan, J. S. CBTRUS Statistical Report: Primary Brain and Other Central Nervous System Tumors Diagnosed in the United States in 2010–2014. *Neuro-Oncol.* **2017**, *19* (Suppl 5), v1–v88. https://doi.org/10.1093/neuonc/nox158.

(2) Ostrom, Q. T.; Cioffi, G.; Gittleman, H.; Patil, N.; Waite, K.; Kruchko, C.; Barnholtz-Sloan, J. S. CBTRUS Statistical Report: Primary Brain and Other Central Nervous System Tumors Diagnosed in the United States in 2012-2016. *Neuro-Oncol.* **2019**, *21* (Suppl 5), v1–v100. https://doi.org/10.1093/neuonc/noz150.

(3) Zhang, A. S.; Ostrom, Q. T.; Kruchko, C.; Rogers, L.; Peereboom, D. M.; Barnholtz-Sloan, J. S. Complete Prevalence of Malignant Primary Brain Tumors Registry Data in the United States Compared with Other Common Cancers, 2010. *Neuro-Oncol.* **2017**, *19* (5), 726–735. https://doi.org/10.1093/neuonc/now252.

(4) Barnholtz-Sloan, J. S.; Ostrom, Q. T.; Cote, D. Epidemiology of Brain Tumors. *Neurol. Clin.* **2018**, *36* (3), 395–419. https://doi.org/10.1016/j.ncl.2018.04.001.

(5) Nayak, L.; Lee, E. Q.; Wen, P. Y. Epidemiology of Brain Metastases. *Curr. Oncol. Rep.* **2012**, *14* (1), 48–54. https://doi.org/10.1007/s11912-011-0203-y.
(6) Louis, D. N.; Ohgaki, H.; Wiestler, O. D.; Cavenee, W. K.; Ellison, D. W.; Figarella-Branger, D.; Perry, A.; Reifenberger, G.; von Deimling, A. *WHO Classification of Tumours of the Central Nervous System. Revised 4th Edition.*; Lyon: IARC, 2016.
(7) Louis, D. N.; Perry, A.; Wesseling, P.; Brat, D. J.; Cree, I. A.; Figarella-Branger, D.; Hawkins, C.; Ng, H. K.; Pfister, S. M.; Reifenberger, G.; Soffietti, R.; von Deimling, A.; Ellison, D. W. The 2021 WHO Classification of Tumors of the Central Nervous System: A Summary. *Neuro-Oncol.* **2021**, *23* (8), 1231–1251. https://doi.org/10.1093/neuonc/noab106.
(8) Hyman, D. M.; Taylor, B. S.; Baselga, J. Implementing Genome-Driven Oncology. *Cell* **2017**, *168* (4), 584–599. https://doi.org/10.1016/j.cell.2016.12.015.
(9) Aldape, K.; Brindle, K. M.; Chesler, L.; Chopra, R.; Gajjar, A.; Gilbert, M. R.; Gottardo, N.; Gutmann, D. H.; Hargrave, D.; Holland, E. C.; Jones, D. T. W.; Joyce, J. A.; Kearns, P.; Kieran, M. W.; Mellinghoff, I. K.; Merchant, M.; Pfister, S. M.; Pollard, S. M.; Ramaswamy, V.; Rich, J. N.; Robinson, G. W.; Rowitch, D. H.; Sampson, J. H.; Taylor, M. D.; Workman, P.; Gilbertson, R. J. Challenges to Curing Primary Brain Tumours. *Nat. Rev. Clin. Oncol.* **2019**, *16* (8), 509–520. https://doi.org/10.1038/s41571-019-0177-5.
(10) Patchell, R. A.; Tibbs, P. A.; Walsh, J. W.; Dempsey, R. J.; Maruyama, Y.; Kryscio, R. J.; Markesbery, W. R.; Macdonald, J. S.; Young, B. A Randomized Trial of Surgery in the Treatment of Single Metastases to the Brain. *N. Engl. J. Med.* **1990**, *322* (8), 494–500. https://doi.org/10.1056/NEJM199002223220802.
(11) Rydzewski, N. R.; Lesniak, M. S.; Chandler, J. P.; Kalapurakal, J. A.; Pollom, E.; Tate, M. C.; Bloch, O.; Kruser, T.; Dalal, P.; Sachdev, S. Gross Total Resection and Adjuvant Radiotherapy Most Significant Predictors of Improved Survival in Patients with Atypical Meningioma. *Cancer* **2018**, *124* (4), 734–742. https://doi.org/10.1002/cncr.31088.
(12) Stupp, R.; Mason, W. P.; van den Bent, M. J.; Weller, M.; Fisher, B.; Taphoorn, M. J. B.; Belanger, K.; Brandes, A. A.; Marosi, C.; Bogdahn, U.; Curschmann, J.; Janzer, R. C.; Ludwin, S. K.; Gorlia, T.; Allgeier, A.; Lacombe, D.; Cairncross, J. G.; Eisenhauer, E.; Mirimanoff, R. O.; European Organisation for Research and Treatment of Cancer Brain Tumor and Radiotherapy Groups; National Cancer Institute of Canada Clinical Trials Group. Radiotherapy plus Concomitant and Adjuvant Temozolomide for Glioblastoma. *N. Engl. J. Med.* **2005**, *352* (10), 987–996. https://doi.org/10.1056/NEJMoa043330.
(13) Brown, T. J.; Brennan, M. C.; Li, M.; Church, E. W.; Brandmeir, N. J.; Rakszawski, K. L.; Patel, A. S.; Rizk, E. B.; Suki, D.; Sawaya, R.; Glantz, M. Association of the Extent of Resection With Survival in Glioblastoma: A Systematic Review and Meta-Analysis. *JAMA Oncol.* **2016**, *2* (11), 1460–1469. https://doi.org/10.1001/jamaoncol.2016.1373.
(14) Smith, J. S.; Chang, E. F.; Lamborn, K. R.; Chang, S. M.; Prados, M. D.; Cha, S.; Tihan, T.; Vandenberg, S.; McDermott, M. W.; Berger, M. S. Role of Extent of Resection in the Long-Term Outcome of Low-Grade Hemispheric Gliomas. *J. Clin. Oncol. Off. J. Am. Soc. Clin. Oncol.* **2008**, *26* (8), 1338–1345. https://doi.org/10.1200/JCO.2007.13.9337.
(15) Stummer, W.; Pichlmeier, U.; Meinel, T.; Wiestler, O. D.; Zanella, F.; Reulen, H.-J.; ALA-Glioma Study Group. Fluorescence-Guided Surgery with 5-Aminolevulinic Acid for Resection of Malignant Glioma: A Randomised Controlled Multicentre Phase III Trial. *Lancet Oncol.* **2006**, *7* (5), 392–401. https://doi.org/10.1016/S1470-2045(06)70665-9.
(16) Molinaro, A. M.; Hervey-Jumper, S.; Morshed, R. A.; Young, J.; Han, S. J.; Chunduru, P.; Zhang, Y.; Phillips, J. J.; Shai, A.; Lafontaine, M.; Crane, J.; Chandra, A.; Flanigan, P.; Jahangiri, A.; Cioffi, G.; Ostrom, Q.; Anderson, J. E.; Badve, C.; Barnholtz-Sloan, J.; Sloan, A. E.; Erickson, B. J.; Decker, P. A.; Kosel, M. L.; LaChance, D.; Eckel-Passow, J.; Jenkins, R.; Villanueva-Meyer, J.; Rice, T.; Wrensch, M.; Wiencke, J. K.; Oberheim Bush, N. A.; Taylor, J.; Butowski, N.; Prados, M.; Clarke, J.; Chang, S.; Chang, E.; Aghi, M.; Theodosopoulos, P.; McDermott, M.; Berger, M. S. Association of Maximal Extent of Resection of Contrast-Enhanced and Non-Contrast-Enhanced Tumor With Survival Within Molecular Subgroups of Patients With Newly Diagnosed Glioblastoma. *JAMA Oncol.* **2020**, *6* (4), 495–503. https://doi.org/10.1001/jamaoncol.2019.6143.
(17) Morris, P. G.; Correa, D. D.; Yahalom, J.; Raizer, J. J.; Schiff, D.; Grant, B.; Grimm, S.; Lai, R. K.; Reiner, A. S.; Panageas, K.; Karimi, S.; Curry, R.; Shah, G.; Abrey, L. E.; DeAngelis, L. M.; Omuro, A. Rituximab, Methotrexate, Procarbazine, and Vincristine Followed by Consolidation Reduced-Dose Whole-Brain Radiotherapy and Cytarabine in Newly Diagnosed Primary CNS Lymphoma: Final Results and Long-Term Outcome. *J. Clin. Oncol. Off. J. Am. Soc. Clin. Oncol.* **2013**, *31* (31), 3971–3979. https://doi.org/10.1200/JCO.2013.50.4910.
(18) Cheng, H.; Chen, B. P.-H.; Soleas, I. M.; Ferko, N. C.; Cameron, C. G.; Hinoul, P. Prolonged Operative Duration Increases Risk of Surgical Site Infections: A Systematic Review. *Surg. Infect.* **2017**, *18* (6), 722–735. https://doi.org/10.1089/sur.2017.089.

(19) Chand, P.; Amit, S.; Gupta, R.; Agarwal, A. Errors, Limitations, and Pitfalls in the Diagnosis of Central and Peripheral Nervous System Lesions in Intraoperative Cytology and Frozen Sections. *J. Cytol. Indian Acad. Cytol.* **2016**, *33* (2), 93–97. https://doi.org/10.4103/0970-9371.182530.

(20) Sarri, B.; Appay, R.; Heuke, S.; Poizat, F.; Franchi, F.; Boissonneau, S.; Caillol, F.; Dufour, H.; Figarella-Branger, D.; Giovaninni, M.; Rigneault, H. Observation of the Compatibility of Stimulated Raman Histology with Pathology Workflow and Genome Sequencing. *Transl. Biophotonics* **2021**, *3* (3). https://doi.org/10.1002/tbio.202000020.

(21) Hollon, T. C.; Pandian, B.; Adapa, A. R.; Urias, E.; Save, A. V.; Khalsa, S. S. S.; Eichberg, D. G.; D'Amico, R. S.; Farooq, Z. U.; Lewis, S.; Petridis, P. D.; Marie, T.; Shah, A. H.; Garton, H. J. L.; Maher, C. O.; Heth, J. A.; McKean, E. L.; Sullivan, S. E.; Hervey-Jumper, S. L.; Patil, P. G.; Thompson, B. G.; Sagher, O.; McKhann, G. M.; Komotar, R. J.; Ivan, M. E.; Snuderl, M.; Otten, M. L.; Johnson, T. D.; Sisti, M. B.; Bruce, J. N.; Muraszko, K. M.; Trautman, J.; Freudiger, C. W.; Canoll, P.; Lee, H.; Camelo-Piragua, S.; Orringer, D. A. Near Real-Time Intraoperative Brain Tumor Diagnosis Using Stimulated Raman Histology and Deep Neural Networks. *Nat. Med.* **2020**, *26* (1), 52–58. https://doi.org/10.1038/s41591-019-0715-9.

(22) Di, L.; Eichberg, D. G.; Huang, K.; Shah, A. H.; Jamshidi, A. M.; Luther, E. M.; Lu, V. M.; Komotar, R. J.; Ivan, M. E.; Gultekin, S. H. Stimulated Raman Histology for Rapid Intraoperative Diagnosis of Gliomas. *World Neurosurg.* **2021**, *150*, e135–e143. https://doi.org/10.1016/j.wneu.2021.02.122.

(23) Eichberg, D. G.; Shah, A. H.; Di, L.; Semonche, A. M.; Jimsheleishvili, G.; Luther, E. M.; Sarkiss, C. A.; Levi, A. D.; Gultekin, S. H.; Komotar, R. J.; Ivan, M. E. Stimulated Raman Histology for Rapid and Accurate Intraoperative Diagnosis of CNS Tumors: Prospective Blinded Study. *J. Neurosurg.* **2019**, 1–7. https://doi.org/10.3171/2019.9.JNS192075.

(24) Rigneault, H.; Berto, P. Tutorial: Coherent Raman Light Matter Interaction Processes. *APL Photonics* **2018**, *3* (9), 091101. https://doi.org/10.1063/1.5030335.

(25) Sarri, B.; Poizat, F.; Heuke, S.; Wojak, J.; Franchi, F.; Caillol, F.; Giovannini, M.; Rigneault, H. Stimulated Raman Histology: One to One Comparison with Standard Hematoxylin and Eosin Staining. *Biomed. Opt. Express* **2019**, *10* (10), 5378–5384. https://doi.org/10.1364/BOE.10.005378.

(26) Heuke, S.; Rimke, I. ngo; Sarri, B.; Gasecka, P.; Appay, R.; Legoff, L.; Volz, P.; Büttner, E.; Rigneault, H. Shot-Noise Limited Tunable Dual-Vibrational Frequency Stimulated Raman Scattering Microscopy. *Biomed. Opt. Express* **2021**, *12* (12), 7780–7789.

(27) Capper, D.; Jones, D. T. W.; Sill, M.; Hovestadt, V.; Schrimpf, D.; Sturm, D.; Koelsche, C.; Sahm, F.; Chavez, L.; Reuss, D. E.; Kratz, A.; Wefers, A. K.; Huang, K.; Pajtler, K. W.; Schweizer, L.; Stichel, D.; Olar, A.; Engel, N. W.; Lindenberg, K.; Harter, P. N.; Braczynski, A. K.; Plate, K. H.; Dohmen, H.; Garvalov, B. K.; Coras, R.; Hölsken, A.; Hewer, E.; Bewerunge-Hudler, M.; Schick, M.; Fischer, R.; Beschorner, R.; Schittenhelm, J.; Staszewski, O.; Wani, K.; Varlet, P.; Pages, M.; Temming, P.; Lohmann, D.; Selt, F.; Witt, H.; Milde, T.; Witt, O.; Aronica, E.; Giangaspero, F.; Rushing, E.; Scheurlen, W.; Geisenberger, C.; Rodriguez, F. J.; Becker, A.; Preusser, M.; Haberler, C.; Bjerkvig, R.; Cryan, J.; Farrell, M.; Deckert, M.; Hench, J.; Frank, S.; Serrano, J.; Kannan, K.; Tsirigos, A.; Brück, W.; Hofer, S.; Brehmer, S.; Seiz-Rosenhagen, M.; Hänggi, D.; Hans, V.; Rozsnoki, S.; Hansford, J. R.; Kohlhof, P.; Kristensen, B. W.; Lechner, M.; Lopes, B.; Mawrin, C.; Ketter, R.; Kulozik, A.; Khatib, Z.; Heppner, F.; Koch, A.; Jouvet, A.; Keohane, C.; Mühleisen, H.; Mueller, W.; Pohl, U.; Prinz, M.; Benner, A.; Zapatka, M.; Gottardo, N. G.; Driever, P. H.; Kramm, C. M.; Müller, H. L.; Rutkowski, S.; von Hoff, K.; Frühwald, M. C.; Gnekow, A.; Fleischhack, G.; Tippelt, S.; Calaminus, G.; Monoranu, C.-M.; Perry, A.; Jones, C.; Jacques, T. S.; Radlwimmer, B.; Gessi, M.; Pietsch, T.; Schramm, J.; Schackert, G.; Westphal, M.; Reifenberger, G.; Wesseling, P.; Weller, M.; Collins, V. P.; Blümcke, I.; Bendszus, M.; Debus, J.; Huang, A.; Jabado, N.; Northcott, P. A.; Paulus, W.; Gajjar, A.; Robinson, G. W.; Taylor, M. D.; Jaunmuktane, Z.; Ryzhova, M.; Platten, M.; Unterberg, A.; Wick, W.; Karajannis, M. A.; Mittelbronn, M.; Acker, T.; Hartmann, C.; Aldape, K.; Schüller, U.; Buslei, R.; Lichter, P.; Kool, M.; Herold-Mende, C.; Ellison, D. W.; Hasselblatt, M.; Snuderl, M.; Brandner, S.; Korshunov, A.; von Deimling, A.; Pfister, S. M. DNA Methylation-Based Classification of Central Nervous System Tumours. *Nature* **2018**, *555* (7697), 469–474. https://doi.org/10.1038/nature26000.

(28) Pekmezci, M.; Morshed, R. A.; Chunduru, P.; Pandian, B.; Young, J.; Villanueva-Meyer, J. E.; Tihan, T.; Sloan, E. A.; Aghi, M. K.; Molinaro, A. M.; Berger, M. S.; Hervey-Jumper, S. L. Detection of Glioma Infiltration at the Tumor Margin Using Quantitative Stimulated Raman Scattering Histology. *Sci. Rep.* **2021**, *11* (1), 12162. https://doi.org/10.1038/s41598-021-91648-8.

(29) Reinecke, D.; von Spreckelsen, N.; Mawrin, C.; Ion-Margineanu, A.; Fürtjes, G.; Jünger, S. T.; Khalid, F.; Freudiger, C. W.; Timmer, M.; Ruge, M. I.; Goldbrunner, R.; Neuschmelting, V. Novel Rapid Intraoperative Qualitative Tumor Detection by a Residual Convolutional Neural Network Using Label-Free Stimulated Raman Scattering Microscopy. *Acta Neuropathol. Commun.* **2022**, *10* (1), 109. https://doi.org/10.1186/s40478-022-01411-x.

(30) Einstein, E. H.; Ablyazova, F.; Rosenberg, A.; Harshan, M.; Wahl, S.; Har-El, G.; Constantino, P. D.; Ellis, J. A.; Boockvar, J. A.; Langer, D. J.; D'Amico, R. S. Stimulated Raman Histology Facilitates Accurate Diagnosis in Neurosurgical Patients: A One-to-One Noninferiority Study. *J. Neurooncol.* **2022**, *159* (2), 369–375. https://doi.org/10.1007/s11060-022-04071-y.
(31) Novis, D. A.; Zarbo, R. J. Interinstitutional Comparison of Frozen Section Turnaround Time. A College of American Pathologists Q-Probes Study of 32868 Frozen Sections in 700 Hospitals. *Arch. Pathol. Lab. Med.* **1997**, *121* (6), 559–567.
(32) Jaafar, H. Intra-Operative Frozen Section Consultation: Concepts, Applications and Limitations. *Malays. J. Med. Sci. MJMS* **2006**, *13* (1), 4–12.
(33) Di, L.; Eichberg, D. G.; Park, Y. J.; Shah, A. H.; Jamshidi, A. M.; Luther, E. M.; Lu, V. M.; Komotar, R. J.; Ivan, M. E.; Gultekin, S. H. Rapid Intraoperative Diagnosis of Meningiomas Using Stimulated Raman Histology. *World Neurosurg.* **2021**, *150*, e108–e116. https://doi.org/10.1016/j.wneu.2021.02.097.

Supplementary Materials: video of 'Live' Stimulated Raman Histology of a central nervous system sample: the video shows the 'Live SRH' operation mode for the microscopic histology exploration of a tumor sample.